Characterization of bottom sediment resuspension events observed in a micro-tidal bay

Manel Grifoll[1,2], Pablo Cerralbo[1,2], Jorge Guillén[3], Manuel Espino[1,2], Lars Boye Hansen[4], Agustín Sánchez-Arcilla[1,2]

[1]Laboratori d'Enginyeria Marítima, Universitat Politècnica de Catalunya (UPC-BarcelonaTech), Barcelona, 08034, Spain
[2]Centre Internacional d'Investigació dels Recursos Costaners (CIIRC), Barcelona, 08034, Spain.
[3]Institut de Ciències del Mar (ICM-CSIC), Barcelona, 08003, Spain.
[4]DHI-Gras, Horsholm, DK-2970, Denmark.

Correspondence to: Manel Grifoll (manel.grifoll@upc.edu)

Abstract. In this study we investigate the variability in near-bottom turbidity in the Alfacs Bay (NW Mediterranean Sea). The bay is characterized by a micro-tidal environment and a relevant seiching activity which may lead to flow velocities of more than 50 cm•s-1. A set of current meters and optical sensors were mounted near the sea bottom to acquire synchronous hydrodynamic and optical information of the water column. The time-series observations showed an evident relation between seiche activity and sediment resuspension events. The observations of turbidity peaks are consistent with the node/anti-node location for the fundamental and first resonance periods of the bay. The implementation of a coupled wave-current numerical model shows a strong spatial variability of the potential resuspension locations. Strong wind events are also a mechanism responsible for the resuspension of fine sediment within the bay. This is confirmed by suspended sediment concentration maps derived from Sentinel-2 satellite imagery. We suggest that the sequence of resuspension events plays a relevant role in suspended sediment concentration, in such a way that the occurrence of sediment resuspension events may increase the suspended sediment in subsequent events. The suspended sediment events likely affect the ecological status of the bay and the sedimentary process in a long-term period.

1 Introduction

Suspended sediment in the water column and subsequent deposition plays a critical role in coastal ecosystems and for managing coastal environments. High levels of suspended sediment concentration in the water column have substantial implications for aquatic ecosystems and natural habitats (Ellis et al., 2002) in particular during large exposure periods (Newcombe and Macdonald, 1991). Furthermore, sediment supplied from rivers potentially transports significant amounts of organic matter, pollutants and heavy metals that may be deposited at the sea bottom or even transported offshore (Palanques et al., 2017). The sediment dynamics is relevant in coastal bays and estuaries due to the large amount of sediment delivered by the freshwater and the potential fine sediment trapping zones. In addition, sediment resuspension contributes significantly to the total nutrient

load (Sondergaard et al., 1992) and prevents sunlight penetration (Mehta, 1989). The analysis and prevention of fine sediment within basins and channels also plays a role for the purposes of port engineering, in order to examine and monitor siltation processes (e.g. Ghosh et al., 2001; van Maren et al., 2015). Finally, the growth of harmful species, such as dinoflagellate cysts, may be related to significant local resuspension through the mixing of the upper layers, resulting in more homogenous cyst profiles in the sediment (Giannakourou et al., 2005).

In coastal areas, sediment transport is related to the hydrodynamic conditions. For long timescales, advection processes determine the final depositional pattern as a function of the sediment and water current variables (Ogston et al., 2000; Bever et al., 2009). Hydrodynamic processes driven by wind waves (Grifoll et al., 2013; Carlin et al., 2016), tides (Fan et al., 2004; Garel et al., 2009), winds (Sherwood et al., 1994; Hofmann et al., 2011), surface seiches (Jordi et al., 2008) or internal-seiches (Shteinman et al., 1997) promote the resuspension, advection and settling of fine sediment, conditioned by the continental sediment sources. Subsequent resuspension effects due to natural causes also contribute to the reworking and final deposition of the sediment load (Guillén et al., 2006; Grifoll et al., 2014a). Moreover, anthropogenic activities such as trawling, ship propellers and waves generated by vessels, bring additional energy in the water system influencing the resuspension, transport and final sediment deposition, in particular in shallow waters (e.g., Garel et al., 2009; Hofmann et al., 2011).

This study focuses on Alfacs Bay (NW Mediterranean Sea; Southern part of the Ebro Delta) which is a micro-tidal estuary. The bay area is intensively exploited by commercial activities, including tourism, fishing and aquaculture, and hence, the ecosystem has a significant economic importance. In the past, the bay has been extensively investigated in terms of its hydrodynamic response (Solé et al., 2009; Llebot et al., 2014; Cerralbo et al., 2015a, 2016, 2018), tidal wave propagation (Cerralbo et al., 2014), biochemical processes (Llebot et al., 2010, 2011) and optical water properties (Ramírez-Pérez et al., 2017). The estuary receives freshwater discharge mainly from the rice fields of the Ebro river. Several episodes of algal blooms have been reported to be linked to increased nutrient concentrations, possibly triggered by resuspension mechanisms. Moreover, the presence of harmful bacteria was found in bivalves with negative effects on aquaculture (Loureiro et al., 2009; Roque et al., 2009).

The goal of this study is to improve knowledge in fine sediment dynamics in coastal bays and provide insight on the controlling factors of sediment resuspension events observed within the Alfacs micro-tidal bay. Using sea-level heights, water currents and wind speed measurements we investigated the driving mechanisms for resuspension of fine bottom sediment within the bay. Subsequently, the spatial and temporal interpretation of the resuspension mechanisms were linked with hydrodynamic processes and analysed, through the implementation of a coupled wave-current numerical model. The contribution aims to explain resuspension mechanisms which may have a positive benefit for management activities (e.g. harmful species resuspension or algal blooms with negative effects on aquaculture activities).

The water circulation in Alfacs Bay has been extensively analysed in previous studies, using observational datasets and numerical models (Camp and Delgado, 1987; Cerralbo et al., 2014, 2015a; Llebot et al., 2014). However, fine sediment dynamics and their resuspension mechanisms have not been examined yet. Synchronous optical measurements, jointly with velocity and sea-level measurements, have facilitated an opportunity to investigate the resuspension mechanisms in Alfacs Bay. Considering the area is a micro-tidal estuary, wind or wind-waves are candidate mechanisms for dispersal of fine sediment.

2 Methods

2.1 Study Area

Alfacs Bay, located in the south of the Ebro delta, is formed by the prograding southern spit. The semi-enclosed bay is approximately 16 km long and 4 km wide. The average depth is 4 m and the maximum depth is about 6.5 m in the middle of the bay (Figure 1). A central channel of 2.5 km in length, 6.5 m deep, connects the bay with the open ocean. Shallow edges of around 1-2 m are found on both sides. To the north, the bay is surrounded by rice fields. From April to December, these fields spill around 10 $m^3 \cdot s^{-1}$ of freshwater loaded with nutrients into the bay. These nutrient rich waters are distributed among several channels, to the eastern side of the delta, close to a sandy beach. The seabed in the central part of the bay is composed of very fine sediments (typically 65-65% silt, 30-35% clay and approximately. 5% sand) with increasing sandy content towards the edges of the bay (Guillén and Palanques, 1997; Satta et al., 2013). The bottom of Alfacs Bay is composed of mud, with a significant content of clay and sand (Palacín et al., 1991). It was discovered that the muddy sediment extended to the central part of the bay, whereas the sand content increased near the spit which separates the bay from the open ocean. The same was found along the southern shallow edge.

The bay is categorised as a salt-wedge estuary (Camp and Delgado, 1987) with almost stable stratification all year. Tidal ranges during spring tides reach around 0.2 m, and the hydrodynamic fluctuations are controlled by the wind modulated by the seiche activity during short periods (Cerralbo et al., 2015a). Both wind and salinity gradients due to freshwater discharge dominate the water circulation in the low-frequency band.(Solé et al., 2009; Cerralbo et al., 2018). Intense regional winds coming from north and northwestern directions together with the orographic effects result in wind jets in the Ebro River valley(Grifoll et al., 2015, 2016). This offshore wind is characterized by noticeable spatial variability due to the surrounding topography (Cerralbo et al., 2015b). The water column within the bay used to be stratified due to the freshwater discharge, but well-mixed conditions are common during winter as a consequence of the hydrodynamic response to strong wind forcing (Llebot et al., 2014) and occasionally to seiches (Cerralbo et al., 2015a). During the summer, the contribution of the temperature at the stratification may also be substantial (Cerralbo et al., 2015a).

2.2 Measurement campaigns

The bulk of the observational data was collected during a 2-month field campaign from July to mid-September 2013. Water currents were measured with two 2MHz Acoustic Doppler Current meter Profilers (ADCPs) moored in the mouth (Fig. 1 - A1) and inner bay (Fig. 1 - A2) and configured to record 10 min averaged data from 10 registers per minute and with 25 cm vertical cells. Both devices were equipped with an Optical Backscatter Sensor (Campbell Scientific OBS-3), a bottom pressure meter and a temperature sensor. The instruments were mounted at the sea bottom in 6.5 m depth, while the sensors were 0.25 m above the sea bed. The signals from the OBS instruments were transformed to the Nephelometric Turbidity Units (NTU) with device calibration report. In the past a linear relation between optical signal and suspended sediment concentration has been observed in the study area (Guillén et al., 2000). The ADCP has a 20 cm blanking zone. Additional sea level data were obtained through a sea level gauge mounted in Sant Carles de la Ràpita harbor (Fig.1) and bottom pressure systems from the ADCPs. Atmospheric data (wind, atmospheric pressure, solar radiation and humidity) were obtained from a land station (M-Sc) located in Sant Carles de la Ràpita, mounted 10 m above the ground.

2.3 Current and wave model implementation

We use the coupled version of SWAN-ROMS models included in the COAWST system in order to simulate the hydrodynamics within the bay. The COAWST system (Warner et al., 2010) consists of several state-of-the-art numerical models that include ROMS (Regional Ocean Modeling System) for ocean and coastal circulation and SWAN (Simulating Waves Nearshore) for surface wind-wave simulation. SWAN is a third-generation numerical wave model that computes random, short-crested waves in coastal regions with shallow water and ambient currents (Booij et al., 1999). It is based on the wave action balance with sources and sinks and incorporates state-of-the-art formulations of the processes of wave generation, dissipation and wave-wave interactions. ROMS is a three-dimensional circulation model which solves the primitive variables on a sigma-level in the vertical and horizontal regular grid. Numerical aspects of ROMS are described in detail in Shchepetkin and McWilliams (2005). In COAWST system, the wave model provides hydrodynamic parameters (i.e., significant wave height, average wave periods, wave propagation direction, near-bottom orbital velocity and wave energy dissipation rate) to the water circulation model. The ocean model provides water depth, sea surface elevation, and current velocity to the wave model. The variables exchange is made “on-line” during the simulation processes, via Model Coupling Toolkit (Jacob et al., 2005), where a multi-processes MPI protocol is used to distribute the computations among several nodes. The COAWST also include different formulations to parametrize the wave-current bottom boundary layer and the wave effect on currents (Warner et al., 2008; Kumar et al., 2012).

The implementation of the COAWST system in Alfacs Bay consists of a regular grid of 186 x 101 points with a spatial resolution of 100 m (in both eastward and northward grid directions) and 12 sigma levels in the vertical direction. Details of the implementation and the skill assessment of the ROMS model in Alfacs Bay is provided by Cerralbo et al. (2015a). The

same regular grid is used by the SWAN model. A two-year water circulation simulation (2012-2013) was performed in order to obtain realistic three-dimensional temperature and salinity fields. The barotropic time step for ROMS is set to 30 s, and in SWAN the wave field is solved in a time interval of 3600 s. The interval time between exchange of variables of ROMS and SWAN was established in 3600 s. For both simulations, water motion at the open boundary was forced by depth-averaged velocities and sea level measurements at A1 (interval data of 600 sec). The freshwater inputs are distributed on 8 points simulating the main rice channels with a total discharge of $10 m^3 s^{-1}$ (Cerralbo et al., 2015a).

The bottom boundary layer was parameterised using the combined wave-current (Styles and Glenn, 2000) adopted in ROMS and SWAN coupling (Warner et al., 2008). The input parameters for the model are the velocity components and wave characteristics near the bottom (wave period, wave direction and the wave orbital direction). For each computational step, an initial assessment of bed roughness length is estimated as a function of the grain size, ripples and sediment transport. Consequnetly, the pure current bottom stress (τ_c) and pure wave bottom stress (τ_w) are computed as:

$$\tau_c = \frac{(u^2+v^2)\kappa^2}{\ln^2(z/z_0)} \quad (1)$$

$$\tau_w = 0.5 f_w u_b^2 \quad (2)$$

where z is the vertical coordinate, z_0 total bottom roughness length, u and v are the water currents components, u_b is the orbital velocity, κ is the von Karman's constant, and f_w is the Madsen wave-friction factor. The maximum bottom stress under wave-current conditions is computed as (Soulsby, 1997):

$$\tau_{wc} = \tau_c \left(1 + 1.2 \left(\frac{\tau_w}{\tau_w+\tau_c}\right)^{1.5}\right) \quad (3)$$

The wave effects from currents are considered using vortex-force formalism, which is included in COAWST. This approach considers the effect from gravity waves on the mean flow, and was tested in different experimental and real configurations by Kumar et al. (2012).

3 Results

3.1 Observations

In order to investigate the suspended sediment events within Alfacs Bay, we used a sub-set of the total observations recorded at A2: from 2nd August to 8th August 2013. This is because the sub-set data selected include the main hydrodynamic conditions susceptible to increase the near-bottom turbidity. Figure 2 shows the time-series recorded at A2 in terms of NTU from the OBS, measured sea level height (additionally sea-level height measured at A1 is also shown), bottom current speed in m•s-1

at A1 and wind speed and direction measured at M-Sc (see Figure 1). The sea level height reference was obtained by subtracting the mean value of the pressure meter time-series provided by the ADCP.

Two typical wind conditions are considered (Figure 2.a and 2.b): sea breeze and the NW winds (Cerralbo et al., 2015a). The sea breeze is associated to an increase of wind speed during the central hours of the day (approximately from 11:00 hr to 18:00 hr with a wind direction within the range of approximately 30º to 180º). From a daily point of view, this seems evident during the 1st to 6th of August. A different pattern is observed during the wind speed peak (7th-8th of August) where 330º wind directions were measured. This corresponds to an offshore wind typical for the region (NW winds called "Mestral").

During the analysis period, a seiche event was also captured on the 3rd of August. This seiche event was previously described hydro-dynamically in Cerralbo et al. (2015a) revealing an oscillation of 1 hour periods in sea-level and currents. This oscillation is characterized by a node (approximately located at A2) where the velocities are maximum, and an anti-node (approximately located at A1) where the amplitude of sea level oscillation is maximum (see sea-level height at A1 in comparison to A2 in Figure 2.c). The homogeneous vertical profile in velocities measured at A2 is shown in Figure 3, with velocity peaks in the order of 0.5 m•s-1 in the water column, at the along-shore direction (i.e. following the axis of the bay). The near-bottom water current speed at A2 (Figure 2.d) show fluctuations with peaks over 0.1 m•s-1, except for the mentioned seiche event where peaks arising 0.4 m•s-1.

The near-bottom turbidity shows a fluctuating behaviour with values ranging from almost zero to over 10 NTU (Figure 2.e). Three differentiated events with high turbidity are observed. These events are E1 (covering from 08:00 of 3rd of August to 10:00 of 5th of August), E2 (03:00 to 12:00 6th of August) and E3 (between 08:00 7th August and 15:00 8th of August). The maximum turbidity is measured during the E1 (maximum turbidity 41.1 NTU). This event lasts for a longer time in comparison to E2 (with a maximum turbidity 4.6 NTU) and E3 (maximum turbidity 12.1 NTU).

3.2 Skill assessment near the sea bottom

The performance of the water circulation model used in this study was examined in terms of sea-level, water currents and temperature/salinity evolution in previous research (Cerralbo et al., 2014). However, in this work we pay attention to the near-bottom velocities due to its relevant role in the sediment resuspension and transport dynamics. Thus, the skill assessment of the near-bottom velocities at A1 and A2 is analysed using a Taylor diagram (Taylor, 2001). This diagram characterizes the similarity between numerical model and observations using their correlation, the Root-Mean-Square Difference (RMSD) and the amplitude of their variations (represented by their standard deviations). The skill of the model improves as the triangles are closer to the observation reference point in the diagram which means the full agreement between the model and the observations (Figure 4). In general, the model results showed a good agreement with the observations in the prevalent along-shelf direction, with correlations larger than 0.5 and RMSD below 1. In addition, the water current fluctuations are well represented in the model because the normalized standard deviation is close to 1 in both measuring points.

3.3 Modelled bottom stress

The bottom stress is obtained from the coupled numerical model implemented in the Alfacs Bay. Figures 5 and 6 show different snapshots of the modelling results to examine the bottom stress pattern for two components (i.e. wave-induced and current-induced bottom stress). These results correspond to different episodes identified from the previous observational analysis. The plot scale of the bottom stress is transformed in log10 for clarity. During the case E1 (3rd of August 2013; 10:00 hr) the bottom stress is mainly caused by currents (Figure 5.left). Maximum values of 0.15 Pa for the combined bottom stress are obtained at the center of the bay, and the mouth. This episode corresponds to a seiche event and the spatial variability of the bottom stress is consistent with the spatial pattern of the node/antinode position. It means that the maximum combined bottom stress (associated with maximum water currents) corresponds to the node position (minimum sea-level amplitude). In contrast, the minimum bottom stress corresponds to the antinode position (maximum sea-level amplitude). The position A2 is located near the node, where the water currents are maximum during the seiche event (0.08 Pa for combined bottom stress). It is worth to mention the node/antinode pattern of the current-induced bottom stress, which presumably would indicate a large spatial variability of the resuspension process within the bay.

After the seiche activity (second stage of E1), the wind speed increases due to the sea-breeze and the current-induced bottom stress (5th of August 2013; 08:00) decreases significantly in particular in the center of the bay (Figure 5.right). The bottom stress distribution shows how the maximum values are obtained near the shoreline (2.2 Pa) due to the contribution of the wave-induced bottom stress. At A2, the combined bottom stress is equal to 0.03 Pa (presumably too small to induce resuspension). For this event, the wave field during the sea-breeze is shown in Figure 7. It reveals that the maximum significant wave height (equal to 0.3 m) occurs near the northern and southern shallow edge consistent with the maximum wave-induced bottom stress.

The bottom-stress pattern during episode E2 (Figure 6.left) is similar to the second stage of episode E1. Both wave and current bottom stress (08:00 7th of August) tends to be small at A2 in comparison to the seiche event. Only substantial bottom stress is observed in the shallow edges of the bay due to the wave action originated by the sea-breeze.

During episode E3 (NW wind, Figure 6.right), the combined bottom stress (23:00 8th of August) is dominated by both wave and current action. The southern part of the bay shows that the maximum wave induced bottom stress is consistent with the wave climate (Figure 7). Also, the current induced bottom stress presents non-negligible values within the bay. Focusing on A2, both mechanisms contribute in a similar manner (wave and current bottom stress is 0.09 and 0.06 Pa respectively) in the combined bottom stress.

4 Discussion

The synchronous time-series of the meteo-oceanographic variables and turbidity shown in Figure 2, joint with the bottom stress model provides a good opportunity to characterize the turbidity peaks measured at A2. During the first stage of episode E1, the bottom current speed responds to the node-antinode pattern with velocities that increase 0.4 m•s-1 at A2. This increase of the bottom velocity caused bottom sediment resuspension and a turbidity peak (Figure 2). Even if an increase of wind speed

occurs (peaks that raise 8 m•s-1), the oscillating pattern of the current (see Figure 3), polarise strongly, following the along-shore direction with 1-hr periods. This suggest an increase of turbidity due to the seiche instead of wind driven current. The analysis of modelled bottom stress during E1 (Figure 5) also suggested that the seiche is the main mechanism for turbidity increase at A2, during the first stage of event E1. Resuspension mechanisms in the water environment caused by seiches is mentioned in observational investigations (Niedda and Greppi, 2007; Chung et al., 2009; Jordi et al., 2011). However, these studies did not explain the high spatial variability of the importance of the seiche-induced resuspension mechanism, which are implied by the modelled current-induced bottom stress. It means observational results about turbidity variability may differ significantly in function of the location of the node/anti-node and its consequent maximum and minimum velocities.

The turbidity still shows large values after the seiche was already dissipated and the bottom current decreased during the second stage of the E1 event. Typical sea-breeze wind conditions were observed (gentle variation of wind direction from 30º to 180º) with a noticeable increase of the wind speed during 4th of August, unrelated to the measured bottom current speed. Llebot et al. (2014) and Cerralbo et al. (2015a) stated that water current profiles due to winds observed in Alfacs Bay does not imply a barotropic shape in the water velocity profiles, suggesting a different behaviour near the bottom, compared to the surface, related to wind set-up phenomena. In consequence, the local resuspension due to wind-breeze seems unlikely at this location of the bay. It seems more feasible that high turbidity measured at A2 during E1 (second stage) is associated to advection of fine sediment resuspended previously by seiche or by sea-breeze activity in the shallow edges of the bay, with a subsequent transport towards the middle of the bay. This last mechanism would also explain the turbidity peak measured during the 5th of August at 00:00; after the fine sediment settling occurred within the bay. The sediment advection within the bay is difficult to confirm according to our data, but Alfacs bathymetry shows a characteristic shallow edge near the coastline (water depths below 2 m; see Figure 1). In these shallow edges the bottom stress increases by 0.8 Pa, suggesting a potential sediment resuspension. The shallow edge may be a source of fine sediment under energetic wind conditions in case of fine sediment availability. In consequence, the advection of resuspended sediment highlights the relevance of the water current patterns within the bay for turbidity measurements.

Episode E2 is attributed to at sea-breeze mechanism. This event is qualitatively less important in terms of turbidity measured at A2. The comparison of the sea-breeze event during 4th of August and 6th of August (both have similar wind and bottom current speed but different turbidity values) seem to indicate the relevance of the previous events and the subsequent advection of fine sediment, following the mechanism explained previously. Similar to the second stage of E1, the bottom stress is low (below 0.02 Pa) in the central basin of the bay; indicating that local resuspension is unlikely. In consequence, the turbidity measured at A2 is probably due to advection processes of suspended sediment from the shallowest areas (combined bottom stress more than 0.8 Pa) in the central basin.

Finally, episode E3 corresponds to a strong NW wind event with wind speeds in excess of 12 m•s-1. The bottom current speed does not show significantly higher values during this episode, in comparison to calm periods. However, in contrast to the sea breeze, the sea waves generated by the NW wind conditions are relevant to the resuspension mechanisms due to an increase of the wave induced bottom stress (Figure 6(right)). Unfortunately, the set-up of the ADCP did not allow us to record the

oscillatory pattern derived from the orbital velocities generated by waves and the relative importance of each resuspension mechanism (i.e. wind or waves) is difficult to quantify.

E2 and E3 are examples of two mechanisms that may increase the turbidity: wind-driven current and wind-waves. In Alfacs Bay, the role of these mechanisms in sediment resuspension is less clear in comparison to seiches because they are a function of wind speed without a correlation between wind module and the turbidity observed. The resuspension of fine sediment due to wind and wind-waves in shallow environments have been reported in literature (Luettich et al., 1990; Ogston et al., 2000; Guillén et al., 2006; Bever et al., 2011; Grifoll et al., 2014b; Hawley et al., 2014; Martyanov and Ryabchenko, 2016; López et al., 2017). Some of this work highlight the complexity of the sediment processes due to the temporal and spatial variability of the importance of resuspension mechanisms and the presence of available material to be resuspended. Apparently, this is the case of our observations, because similar wind conditions do not imply the same turbidity measurements. A good example is the sea-breeze wind events during 4th, 5th and 6th of August in which different turbidity values were observed. As mentioned in the previous section, advective fluxes and the sequence of events may have a relevant role in the observed water turbidity. Many authors have reported an apparent influence on advective fluxes correlated with suspended sediment concentration after an initial deposition of fine sediment (Sherwood et al., 1994; Ogston et al., 2000; Guillén et al., 2006; Harris et al., 2008; Bever et al., 2009; Grifoll et al., 2014b). This means that on longer timescales, advection of sediment by currents may redistribute sediment and determine final deposition patterns (Wright and Nittrouer, 1995). This may be the mechanism responsible of high turbidity observed under relatively low hydrodynamic conditions. For instance, the sea-breeze event of 2nd August does not cause high turbidity, in contrast to the event on 5th of August (second stage of E1 event), which may indicate that an energetic event (i.e. seiche) could mobilise sediment, which is resuspended easily in subsequent events. The lack of proportionality of the resuspension related to hydrodynamics is also found in extended data time-series where divergences are associated mainly to sediment availability in the bottom, among other factors (e.g. in Wiberg et al. (1994) or López et al. (2017)). In the case of Alfacs Bay, more extended observations may clarify the relation between wind intensity, wind-waves, seiches and the amount of suspended sediment and fluxes taking into account the sequence of energetic events.

The sediment distribution in Alfacs Bay (high percentage of silt and clay in the central basin and sand prevalence in the southern, eastern and western shore) is consistent with the modeling results shown in this study, where larger bottom stress were obtained in the lateral shallow edges due to the contribution of the wave induced bottom stress in shallow areas. However, the deposition mechanism is a complex process, composed from an initial settling and a subsequent dispersal, as described in (Wright and Nittrouer, 1995). Further sediment transport simulations, including those considering sediment classes and erosion and settling effects, would help to investigate the sediment settling dynamics and its final deposition. These processes should include the cohesive nature of the fine sediment or other phenomena's, such as armouring or bioturbation, that may modify the physical properties of the sediment layers (van Ledden et al., 2004; Amoudry and Souza, 2011).

The characteristics of the bay, such as the relative narrow and shallow entrance, favour the trapping of fine sediments, fed either by the freshwater outflow or the exchange between the open sea and the inner bay. The trapping effect of the bay may entail the presence of a thin surface bottom layer of fine sediment easily subject to resuspension. This behaviour is typical

from shallow and sheltered environments such as lagoons or lakes. According to Luettich et al. (1990) and Hofmann et al. (2011), the regular resuspension events in sheltered and shallow water bodies prevents sediment consolidation and formation of a cohesive sediment layer. This could explain the high turbidity values observed in the Alfacs Bay under relatively weak conditions, such as sea-breeze events, which would likely not occur if the sediment was cohesive.

The Sentinel-2 satellites provide imagery which allow for further identification of scenarios with resuspension linked to hydrodynamic forcing. Figure 8 shows the Total Suspended Matter (TSM in mgr•l-1) for the Alfacs Bay in two differentiate scenarios: NW wind and Calm conditions. Without access to local calibration data, a generalized approach for TSM retrieval has been applied. Through SNAP (v. 6.0.0) the Level 1C Sentinel-2 MSI data was converted to geophysical values (suspended sediment concentration) using the most recent version of the water quality processor 'C2RCC' (v. 1.0). The C2RCC processor was run using default values. Following processing in SNAP the data was post-processed (tiles merged, and data noise corrected) and the TSM maps created. NW wind conditions increase the TSM substantially in the southeastern shallow edges. This would be a source of a subsequent advection of fine sediment towards the central bay as it was stated in the previous paragraphs. In contrast, the values of TSM decrease significantly during calm conditions.

Also, the proximity of the Ebro river mouth (15 km at north) may increase the suspended sediment within the bay under specific circumstances. River discharge is the main driver of the Ebro River plume, followed by wind and regional oceanic circulation that tend to be southward (Fernández-Nóvoa et al., 2015; Mestres et al., 2003). Analysis of the turbid plume by remote sensing products indicate that more than 70% of the plume extension was located south of the river mouth, influenced by the regional oceanic circulation (Fernández-Nóvoa et al., 2015). Other external sediment sources may be associated with freshwater discharge from channels, overwash in the bar, flash flood from small creeks or aeolian transport. The complete study of the suspended sediment dynamics will provide objective information to address the problem of degrading water quality within the bay and how to make use of natural mechanisms to limit undesired concentrations of nutrients or pollutants. This applies in particular to harmful algae blooms prone to occur in the area under present and future conditions.

5 Conclusions

The observational set and the wave-current numerical results obtained for Alfacs Bay have allowed for a thorough investigation of the resuspension mechanisms of fine sediment. The results indicate evidence of a clear mechanism of resuspension induced by eventual seiche events, which according to the bottom stress patterns may have a relevant spatial variability within the bay consistent with the node/anti-node position. The wind and wind-wave mechanisms are also responsible for fine sediment resuspension during energetic wind events, especially in shallow areas of the bay. A similar contribution of current-induced bottom stress and wave-induced bottom stress in the assessment of the combined wave-current bottom stress is found for the NW wind case. In the case of the sea breeze, the wave-induced bottom stress prevails. The lack of proportionality between the turbidity and hydrodynamic highlights the relevance of the sequence of the events suggesting an effect of advective sediment fluxes within the bay (from the lateral shallow edges to the middle of the bay) which increase the suspended sediment

concentration. The trapping effect of the bay may entail the presence of a thin surface layer of fine sediment, easily involved in resuspension neglecting the expected cohesive effects. However, these points deserve further analysis with extended data sets and sediment transport modeling. The exchange of fine sediment within the bay and the open sea is also evident according to remote sensing images. However, these points deserve further analysis with extended data sets and sediment transport modeling. As a region with high-anthropogenic pressure, this research may contribute to develop integrated development plans considering sustainable aquaculture activities and climate change mitigation in the Ebro Delta.

Acknowledgments

The authors are grateful for the collaboration IRTA staff for the participation in the field campaigns carried out within the framework of the monitoring program of water quality at the shellfish growing areas in Catalonia. Thanks to the data provided by Puertos del Estado and AEMET. This work received funding from the EU H2020 program under grant agreement no. 730030 (CEASELESS project). We also want to thank to Secretaria d'Universitats i Recerca del Dpt. d'Economia i Coneixement de la Generalitat de Catalunya (Ref 2014SGR1253) who support our research group. The paper contains modified Copernicus Sentinel data [2017/2018].

References

Amoudry, L. O. and Souza, A. J.: Deterministic coastal morphological and sediment transport modeling: a review and discussion, Rev. Geophys., (49), 1–21, doi:10.1029/2010RG000341.1.INTRODUCTION, 2011.

Bever, A. J., Harris, C. K., Sherwood, C. R. and Signell, R. P.: Deposition and flux of sediment from the Po River, Italy: An idealized and wintertime numerical modeling study, Mar. Geol., 260(1–4), 69–80, doi:10.1016/j.margeo.2009.01.007, 2009.

Bever, A. J., McNinch, J. E. and Harris, C. K.: Hydrodynamics and sediment-transport in the nearshore of Poverty Bay, New Zealand: Observations of nearshore sediment segregation and oceanic storms, Cont. Shelf Res., 31(6), 507–526, doi:10.1016/j.csr.2010.12.007, 2011.

Booij, N., Ris, R. C. and Holthuijsen, L. H.: A third-generation wave model for coastal regions: 1. Model description and validation, J. Geophys. Res., 104(C4), 7649, doi:10.1029/98JC02622, 1999.

Camp, J. and Delgado, M.: Hidrografía de las bahías del delta del Ebro, Investig. Pesq., 51(3), 351–369, 1987.

Carlin, J. A., Lee, G. hong, Dellapenna, T. M. and Laverty, P.: Sediment resuspension by wind, waves, and currents during meteorological frontal passages in a micro-tidal lagoon, Estuar. Coast. Shelf Sci., 172, 24–33, doi:10.1016/j.ecss.2016.01.029, 2016.

Cerralbo, P., Grifoll, M., Valle-Levinson, A. and Espino, M.: Tidal transformation and resonance in a short, microtidal Mediterranean estuary (Alfacs Bay in Ebre delta), Estuar. Coast. Shelf Sci., 145, doi:10.1016/j.ecss.2014.04.020, 2014.

Cerralbo, P., Grifoll, M. and Espino, M.: Hydrodynamic response in a microtidal and shallow bay under energetic wind and

seiche episodes, J. Mar. Syst., 149, doi:10.1016/j.jmarsys.2015.04.003, 2015a.

Cerralbo, P., Grifoll, M., Moré, J., Bravo, M., Sairouní Afif, a. and Espino, M.: Wind variability in a coastal area (Alfacs Bay, Ebro River delta), Adv. Sci. Res., 12, 11–21, doi:10.5194/asr-12-11-2015, 2015b.

Cerralbo, P., Espino, M. and Grifoll, M.: Modeling circulation patterns induced by spatial cross-shore wind variability in a small-size coastal embayment, Ocean Model., 104, doi:10.1016/j.ocemod.2016.05.011, 2016.

Cerralbo, P., Espino, M., Grifoll, M., and Valle-Levinsion, A: Subtidal circulation in a microtidal Mediterranean bay, Sci. Mar. 82(4): 231-243, doi:10.3989/scimar.4801.16A, 2018.

Chung, E. G., Bombardelli, F. A. and Schladow, S. G.: Sediment resuspension in a shallow lake, Water Resour. Res., 45(5), 1–18, doi:10.1029/2007WR006585, 2009.

Ellis, J., Cummings, V., Hewitt, J., Thrush, S. and Norkko, A.: Determining effects of suspended sediment on condition of a suspension feeding bivalve (Atrina zelandica): Results of a survey, a laboratory experiment and a field transplant experiment, J. Exp. Mar. Bio. Ecol., 267(2), 147–174, doi:10.1016/S0022-0981(01)00355-0, 2002.

Fan, S., Swift, D. J. P., Traykovski, P., Bentley, S., Borgeld, J. C., Reed, C. W. and Niedoroda, A. W.: River flooding, storm resuspension, and event stratigraphy on the northern California shelf: observations compared with simulations, Mar. Geol., 210(1–4), 17–41, doi:10.1016/j.margeo.2004.05.024, 2004.

Fernández-Nóvoa, D., Mendes, R., deCastro, M., Dias, J. M., Sánchez-Arcilla, A. and Gómez-Gesteira, M.: Analysis of the influence of river discharge and wind on the Ebro turbid plume using MODIS-Aqua and MODIS-Terra data, J. Mar. Syst., 142, 40–46, doi:10.1016/j.jmarsys.2014.09.009, 2015.

Garel, E., Pinto, L., Santos, A. and Ferreira, Ó.: Tidal and river discharge forcing upon water and sediment circulation at a rock-bound estuary (Guadiana estuary, Portugal), Estuar. Coast. Shelf Sci., 84(2), 269–281, doi:10.1016/j.ecss.2009.07.002, 2009.

Ghosh, L. K., Prasad, N., Joshi, V. B. and Kunte, S. S.: A study on siltation in access channel to a port, Coast. Eng., 43(1), 59–74, doi:10.1016/S0378-3839(01)00006-0, 2001.

Giannakourou, A., Orlova, T. Y., Assimakopoulou, G. and Pagou, K.: Dinoflagellate cysts in recent marine sediments from Thermaikos Gulf, Greece: Effects of resuspension events on vertical cyst distribution, Cont. Shelf Res., 25(19–20), 2585–2596, doi:10.1016/j.csr.2005.08.003, 2005.

Grifoll, M., Gracia, V., Fernandez, J. and Espino, M.: Suspended sediment observations in the Barcelona inner-shelf during storms, J. Coast. Res., (SPEC. ISSUE 65), doi:10.2112/SI65-259, 2013.

Grifoll, M., Gracia, V., Aretxabaleta, A. L., Guillén, J., Espino, M. and Warner, J. C.: Formation of fine sediment deposit from a flash flood river in the Mediterranean Sea, J. Geophys. Res. Ocean., 119, 5837–5853, doi:10.1002/2014JC010187, 2014a.

Grifoll, M., Gracia, V., Aretxabaleta, A., Guillén, J., Espino, M. and Warner, J. C.: Formation of fine sediment deposit from a flash flood river in the Mediterranean Sea, J. Geophys. Res. C Ocean., 119(9), doi:10.1002/2014JC010187, 2014b.

Grifoll, M., Aretxabaleta, A. L. and Espino, M.: Shelf response to intense offshore wind, J. Geophys. Res. C Ocean., 120(9), 6564–6580, doi:10.1002/2015JC010850, 2015.

Grifoll, M., Navarro, J., Pallares, E., Ràfols, L., Espino, M. and Palomares, A.: Ocean–atmosphere–wave characterisation of a wind jet (Ebro shelf, NW Mediterranean Sea), Nonlinear Process. Geophys., 23(3), 143–158, doi:10.5194/npg-23-143-2016, 2016.

Guillen, J. and Palanques, A.: A shoreface zonation in the Ebro Delta based on grain size distribution, J. Coast. Res., 13(3), 867–878 [online] Available from: http://www.scopus.com/inward/record.url?eid=2-s2.0-0030746817&partnerID=tZOtx3y1, 1997.

Guillén, J., Palanques, a, Puig, P. and Durrieu de Madron, X.: Field calibration of optical sensors for measuring suspended sediment concentration in the western Mediterranean, Sci. Mar., 64(4), 427–435, doi:10.3989/scimar.2000.64n4427, 2000.

Guillén, J., Bourrin, F., Palanques, a., Durrieu de Madron, X., Puig, P. and Buscail, R.: Sediment dynamics during wet and dry storm events on the Têt inner shelf (SW Gulf of Lions), Mar. Geol., 234(1–4), 129–142, doi:10.1016/j.margeo.2006.09.018, 2006.

Harris, C. K., Sherwood, C. R., Signell, R. P., Bever, A. J. and Warner, J. C.: Sediment dispersal in the northwestern Adriatic Sea, J. Geophys. Res., 113(C11), C11S03, doi:10.1029/2006JC003868, 2008.

Hawley, N., Redder, T., Beletsky, R., Verhamme, E., Beletsky, D. and DePinto, J. V.: Sediment resuspension in Saginaw Bay, J. Great Lakes Res., 40(S1), 18–27, doi:10.1016/j.jglr.2013.11.010, 2014.

Hofmann, H., Lorke, A. and Peeters, F.: Wind and ship wave-induced resuspension in the littoral zone of a large lake, Water Resour. Res., 47(9), 1–12, doi:10.1029/2010WR010012, 2011.

Jacob, R., Larson, J. and and Ong, E.: {M}\cdotn communication and parallel interpolation in {CCSM3} using the {M}odel {C}oupling {T}oolkit, Int. J. High Perf. Comp. App., 19, 293–308, 2005.

Jordi, A., Basterretxea, G., Casas, B., Anglès, S. and Garcés, E.: Seiche-forced resuspension events in a Mediterranean harbour, Cont. Shelf Res., 28(4–5), 505–515, doi:10.1016/j.csr.2007.10.009, 2008.

Jordi, A., Basterretxea, G. and Wang, D.-P.: Local versus remote wind effects on the coastal circulation of a microtidal bay in the Mediterranean Sea, J. Mar. Syst., 88(2), 312–322 [online] Available from: http://www.sciencedirect.com/science/article/pii/S0924796311001266, 2011.

Kumar, N., Voulgaris, G., Warner, J. C. and Olabarrieta, M.: Implementation of the vortex force formalism in the coupled ocean-atmosphere-wave-sediment transport (COAWST) modeling system for inner shelf and surf zone applications, Ocean Model., 47, 65–95, doi:10.1016/j.ocemod.2012.01.003, 2012.

van Ledden, M., van Kesteren, W. G. . and Winterwerp, J. .: A conceptual framework for the erosion behaviour of sand–mud mixtures, Cont. Shelf Res., 24(1), 1–11, doi:10.1016/j.csr.2003.09.002, 2004.

Llebot, C., Spitz, Y. H., Sol??, J. and Estrada, M.: The role of inorganic nutrients and dissolved organic phosphorus in the phytoplankton dynamics of a Mediterranean bay: A modeling study, J. Mar. Syst., 83(3–4), 192–209, doi:10.1016/j.jmarsys.2010.06.009, 2010.

Llebot, C., Solé, J., Delgado, M., Fernández-Tejedor, M., Camp, J. and Estrada, M.: Hydrographical forcing and phytoplankton variability in two semi-enclosed estuarine bays, J. Mar. Syst., 86(3–4), 69–86, doi:10.1016/j.jmarsys.2011.01.004, 2011.

Llebot, C., Rueda, F. J., Solé, J., Artigas, M. L. and Estrada, M.: Hydrodynamic states in a wind-driven microtidal estuary (Alfacs Bay), J. Sea Res., 85, 263–276, doi:10.1016/j.seares.2013.05.010, 2014.

López, L., Guillén, J., Palanques, A. and Grifoll, M.: Seasonal sediment dynamics on the Barcelona inner shelf (NW Mediterranean): A small Mediterranean river- and wave-dominated system, Cont. Shelf Res., 145, doi:10.1016/j.csr.2017.07.008, 2017.

Loureiro, S., Garcés, E., Fernández-Tejedor, M., Vaqué, D. and Camp, J.: Pseudo-nitzschia spp. (Bacillariophyceae) and dissolved organic matter (DOM) dynamics in the Ebro Delta (Alfacs Bay, NW Mediterranean Sea), Estuar. Coast. Shelf Sci., 83(4), 539–549, doi:10.1016/j.ecss.2009.04.029, 2009.

Luettich, R. A. J., Harleman, D. R. F. and Somlyódy, L.: Dynamic behavior of suspended sediment concentrations in a shallow lake perturbed by episodic wind events, Limnol. Oceanogr., 35(5), 1050–1067, doi:10.4319/lo.1990.35.5.1050, 1990.

van Maren, D. S., van Kessel, T., Cronin, K. and Sittoni, L.: The impact of channel deepening and dredging on estuarine sediment concentration, Cont. Shelf Res., 95, 1–14, doi:10.1016/j.csr.2014.12.010, 2015.

Martyanov, S. and Ryabchenko, V.: Bottom sediment resuspension in the easternmost Gulf of Finland in the Baltic Sea: A case study based on three-dimensional modeling, Cont. Shelf Res., 117, 126–137, doi:10.1016/j.csr.2016.02.011, 2016.

Mehta, A. J.: On estuarine cohesive sediment suspension behavior, J. Geophys. Res. Ocean., 94(C10), 14303–14314, doi:10.1029/JC094iC10p14303, 1989.

Mestres, M., Sierra, J. P. A. U., Sánchez-Arcilla, A., González, J., Río, D. E. L., Wolf, T. and Rodríguez, A.: Modelling of the Ebro River plume . Validation with field observations, Scientia Marina, 67(4), 379–391, 2003.

Newcombe, C. P. and Macdonald, D. D.: Effects of Suspended Sediments on Aquatic Ecosystems, North Am. J. Fish. Manag., 11(1), 72–82, doi:10.1577/1548-8675(1991)011<0072:EOSSOA>2.3.CO;2, 1991.

Niedda, M. and Greppi, M.: Tidal, seiche and wind dynamics in a small lagoon in the Mediterranean Sea, Estuar. Coast. Shelf Sci., 74(1–2), 21–30, doi:10.1016/j.ecss.2007.03.022, 2007.

Ogston, A. ., Cacchione, D. ., Sternberg, R. . and Kineke, G. .: Observations of storm and river flood-driven sediment transport on the northern California continental shelf, Cont. Shelf Res., 20(16), 2141–2162, doi:10.1016/S0278-4343(00)00065-0, 2000.

Palacín, C., Martin, D. and and Gili, J. M.: Features of spatial distribution of benthic infauna in a Mediterranean shallow-water Bay, Mar. Biol., 321, 315–321, 1991.

Palanques, A., Lopez, L., Guillén, J., Puig, P. and Masqué, P.: Decline of trace metal pollution in the bottom sediments of the Barcelona City continental shelf (NW Mediterranean), Sci. Total Environ., 579, 755–767, doi:10.1016/j.scitotenv.2016.11.031, 2017.

Ramírez-Pérez, M., Gonçalves-Araujo, R., Wiegmann, S., Torrecilla, E., Bardaji, R., Röttgers, R., Bracher, A. and Piera, J.: Towards cost-effective operational monitoring systems for complex waters: Analyzing small-scale coastal processes with optical transmissometry, PLoS One, 12(1), 1–21, doi:10.1371/journal.pone.0170706, 2017.

Roque, A., Lopez-Joven, C., Lacuesta, B., Elandaloussi, L., Wagley, S., Furones, M. D., Ruiz-Zarzuela, I., De Blas, I., Rangdale, R. and Gomez-Gil, B.: Detection and identification of tdh- And trh-positive Vibrio parahaemolyticus strains from

four species of cultured bivalve molluscs on the Spanish Mediterranean coast, Appl. Environ. Microbiol., 75(23), 7574–7577, doi:10.1128/AEM.00772-09, 2009.

Satta, C. T., Anglès, S., Lugliè, A., Guillén, J., Sechi, N., Camp, J. and Garcés, E.: Studies on dinoflagellate cyst assemblages in two estuarine Mediterranean bays: A useful tool for the discovery and mapping of harmful algal species, Harmful Algae, 24, 65–79, doi:10.1016/j.hal.2013.01.007, 2013.

Shchepetkin, A. F. and McWilliams, J. C.: The regional oceanic modeling system (ROMS): a split-explicit, free-surface, topography-following-coordinate oceanic model, Ocean Model., 9(4), 347–404, doi:10.1016/j.ocemod.2004.08.002, 2005.

Sherwood, C. R., Butman, B., Cacchione, D. A., Drake, D. E., Gross, T. F., Sternberg, R. W., Wiberg, P. L. and Williams, A. J.: Sediment-transport events on the northern California continental shelf during the 1990–1991 STRESS experiment, Cont. Shelf Res., 14(10–11), 1063–1099, doi:10.1016/0278-4343(94)90029-9, 1994.

Shteinman, B., Eckert, W., Kaganowsky, S. and Zohary, T.: Seiche-Induced Resuspension in Lake Kinneret: A Fluorescent Tracer Experiment, in The Interactions Between Sediments and Water: Proceedings of the 7th International Symposium, Baveno, Italy 22--25 September 1996, edited by R. D. Evans, J. Wisniewski, and J. R. Wisniewski, pp. 123–131, Springer Netherlands, Dordrecht., 1997.

Solé, J., Turiel, A., Estrada, M., Llebot, C., Blasco, D., Camp, J., Delgado, M., Fernández-Tejedor, M. and Diogène, J.: Climatic forcing on hydrography of a Mediterranean bay (Alfacs Bay), Cont. Shelf Res., 29(15), 1786–1800, doi:10.1016/j.csr.2009.04.012, 2009.

Sondergaard, M., Kristensen, P. and Jeppesen, E.: Phosphorus release from ressuspended sediment in the shallow and wind-exposed Lake Arreso, Denmark, Hydrobiologia, 228, 91–99, 1992.

Soulsby, R.: Dynamics of marine sands, Thomas Telford Publishing., 1997.

Styles, R. and Glenn, S. M.: Modeling stratified wave and current bottom boundary layers on the continental shelf, J. Geophys. Res., 105(C10), 24119–24139, doi:10.1029/2000JC900115, 2000.

Taylor, K. E.: Summarizing multiple aspects of model performance in a single diagram, J. Geophys. Res., 106(D7), 7183–7192, doi:10.1029/2000JD900719, 2001.

Warner, J. C., Sherwood, C. R., Signell, R. P., Harris, C. K. and Arango, H. G.: Development of a three-dimensional, regional, coupled wave, current, and sediment-transport model, Comput. Geosci., 34(10), 1284–1306, doi:10.1016/j.cageo.2008.02.012, 2008.

Warner, J. C., Armstrong, B., He, R. and Zambon, J. B.: Development of a Coupled Ocean–Atmosphere–Wave–Sediment Transport (COAWST) Modeling System, Ocean Model., 35(3), 230–244, doi:10.1016/j.ocemod.2010.07.010, 2010.

Wiberg, P. L., Drake, D. E. and Cacchione, D. A.: Sediment resuspension and bed armoring during high bottom stress events on the northern California inner continental shelf: measurements and predictions, Cont. Shelf Res., 14(10), 1191–1219, doi:http://dx.doi.org/10.1016/0278-4343(94)90034-5, 1994.

Wright, L. D. and Nittrouer, C. a.: Dispersal of River Sediments in Coastal Seas: Six Contrasting Cases, Estuaries, 18(3), 494, doi:10.2307/1352367, 1995.

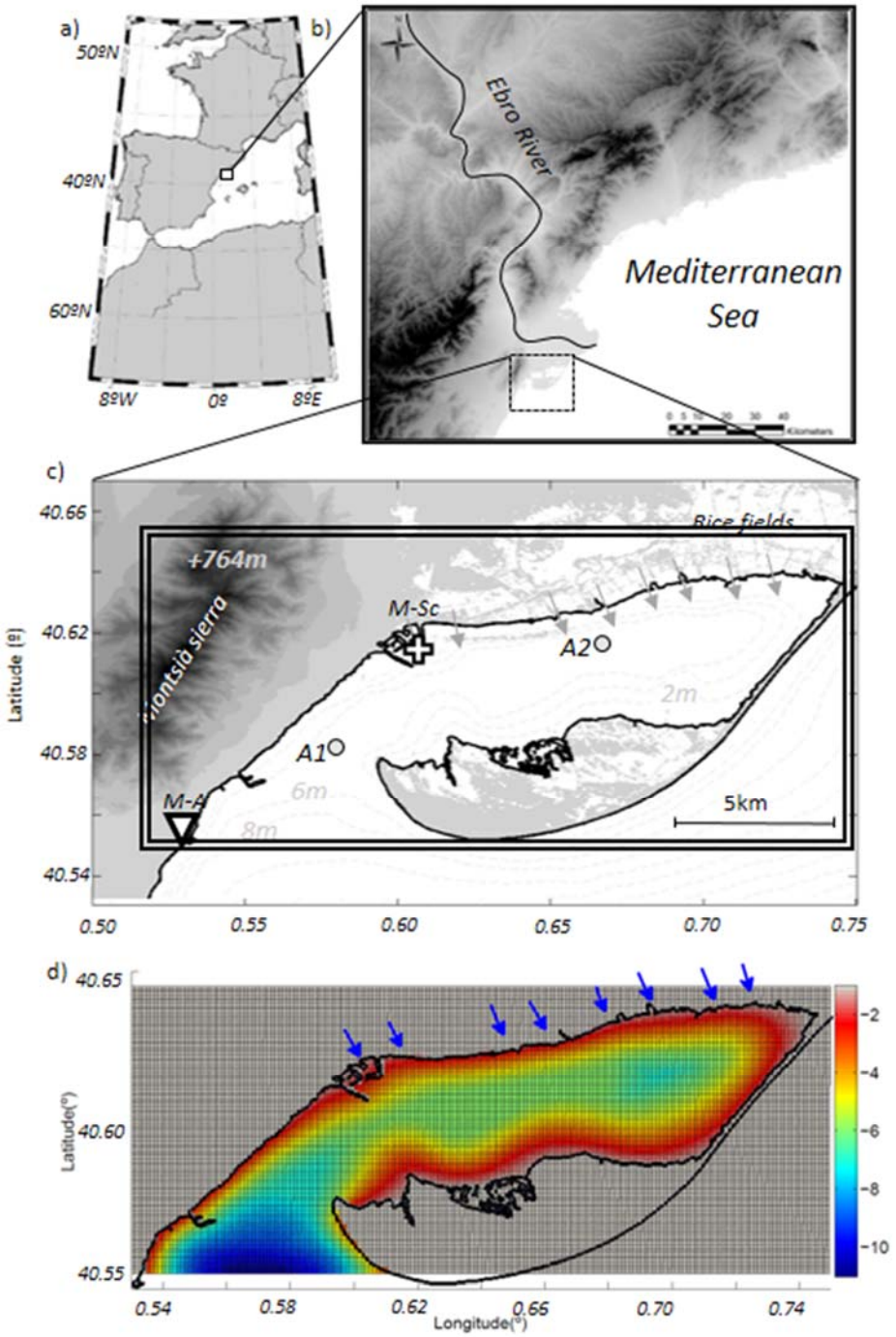

490 Figure 1: **a: Location of the Ebro River Delta in a regional context; b: Location of the Alfacs Bay in the Ebro River Delta; c: Overview map of the Alfacs Bay. The location of the meteorological station is marked with a triangle (M-A) and a white cross marks the location of the Sant Carles de la Ràpita tide gauge (M-Sc). The Grey circles show the ADCP and OBS mooring locations A1 and A2, respectively. The gray arrows at the northern coast depict the freshwater drainage points considered in the simulation;**

d: d The figure shows the modelling domain with the background grid corresponding to the numerical mesh used in the numerical model. The blue arrows on the northern coast show the freshwater drainage points considered in the simulation. The colourbar indicates depth in meters.

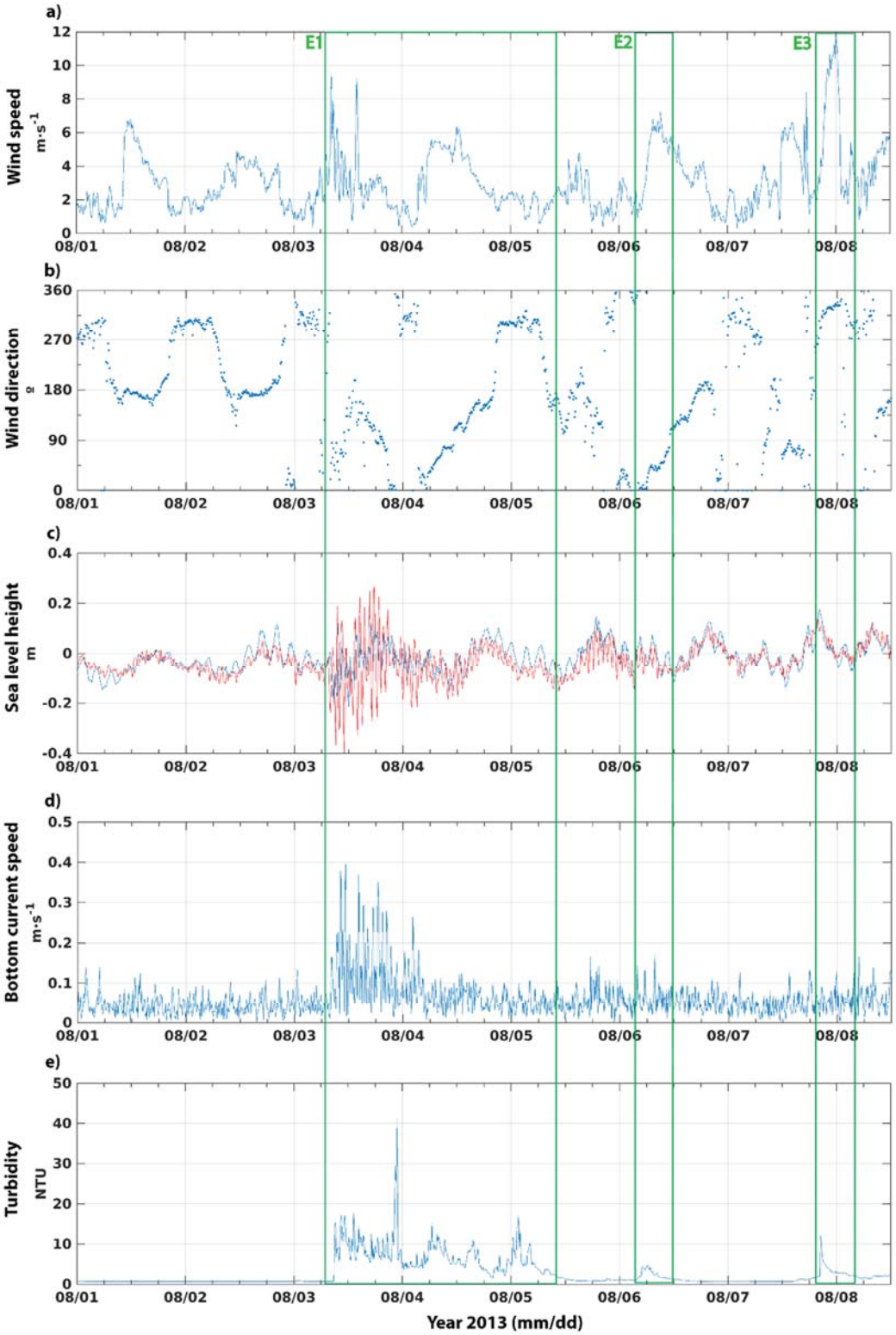
a)
Wind speed
m·s-1
E1
E2
E3
b)
Wind direction
°
c)
Sea level height
m
d)
Bottom current speed
m·s-1
e)
Turbidity
NTU
08/01
08/02
08/03
08/04
08/05
08/06
08/07
08/08
Year 2013 (mm/dd)

Figure 2: Time-series of the variables measured during the field campaign. (a) wind speed measured at M-Sc. (b) wind direction measured at M-Sc. (c) Sea-level height measured at A2 (blue) and A1 (red). (d) near-bottom current speed measured at A1. (e) NTU measured by OBS mounted at the A2 station. Vertical bars show the episodes considered in the analysis.

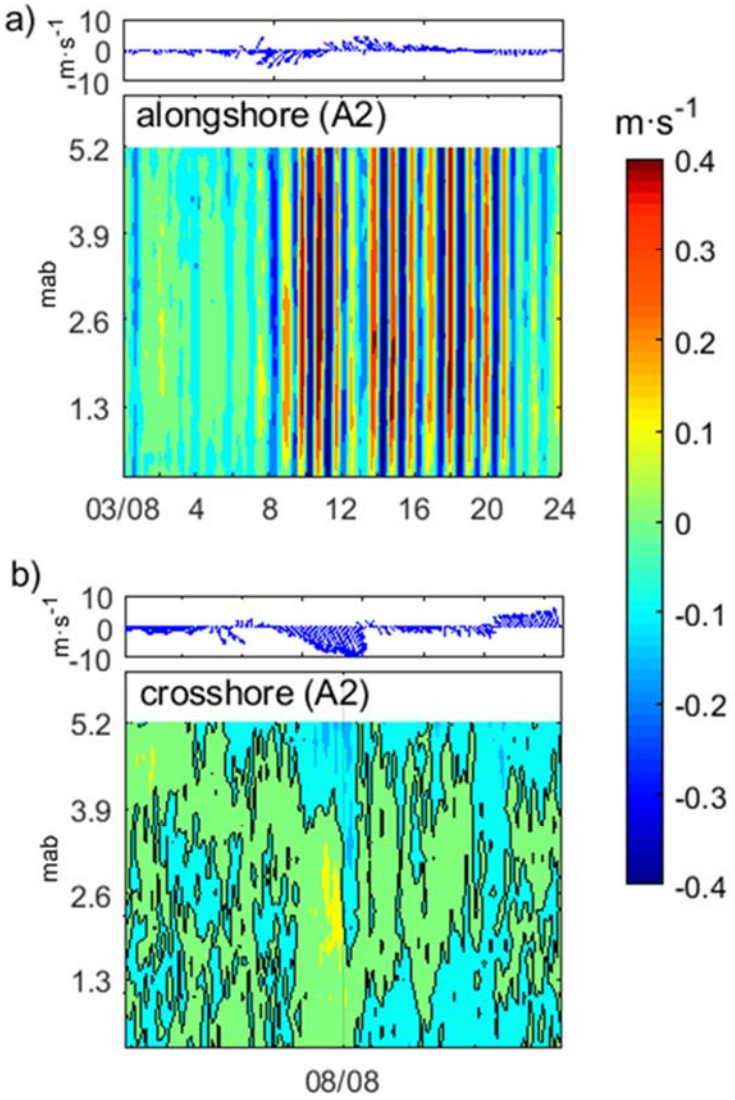

Figure 3: Each panel shows on the top the wind speed measured at M-Sc in $m \cdot s^{-1}$. At the bottom the vertical profiles show the speed measured at A2 (in $m \cdot s^{-1}$; mab stands for meters above the bottom). Black lines show 0 speed isolines. In each panel, different events are shown: a) 2013/8/3 for the along-shore direction and b) as (a) but for the cross-shore direction on 2013/8/8.

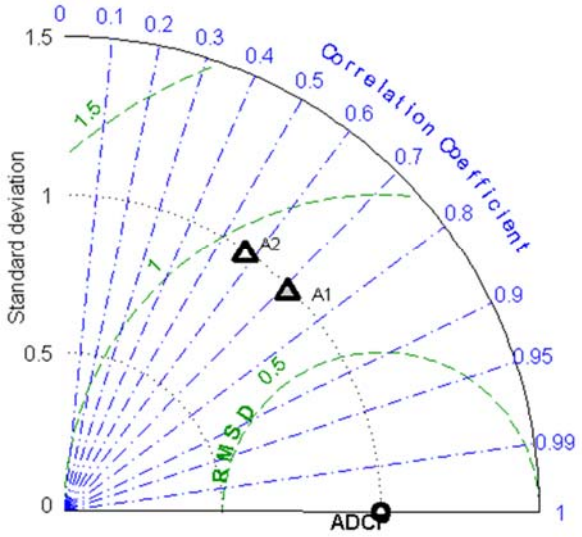

505

Figure 4: Taylor diagram comparing the error metrics between the observations and model results for the near-bottom currents. A1 and A2 correspond to the ADCP locations shown in Figure 1.

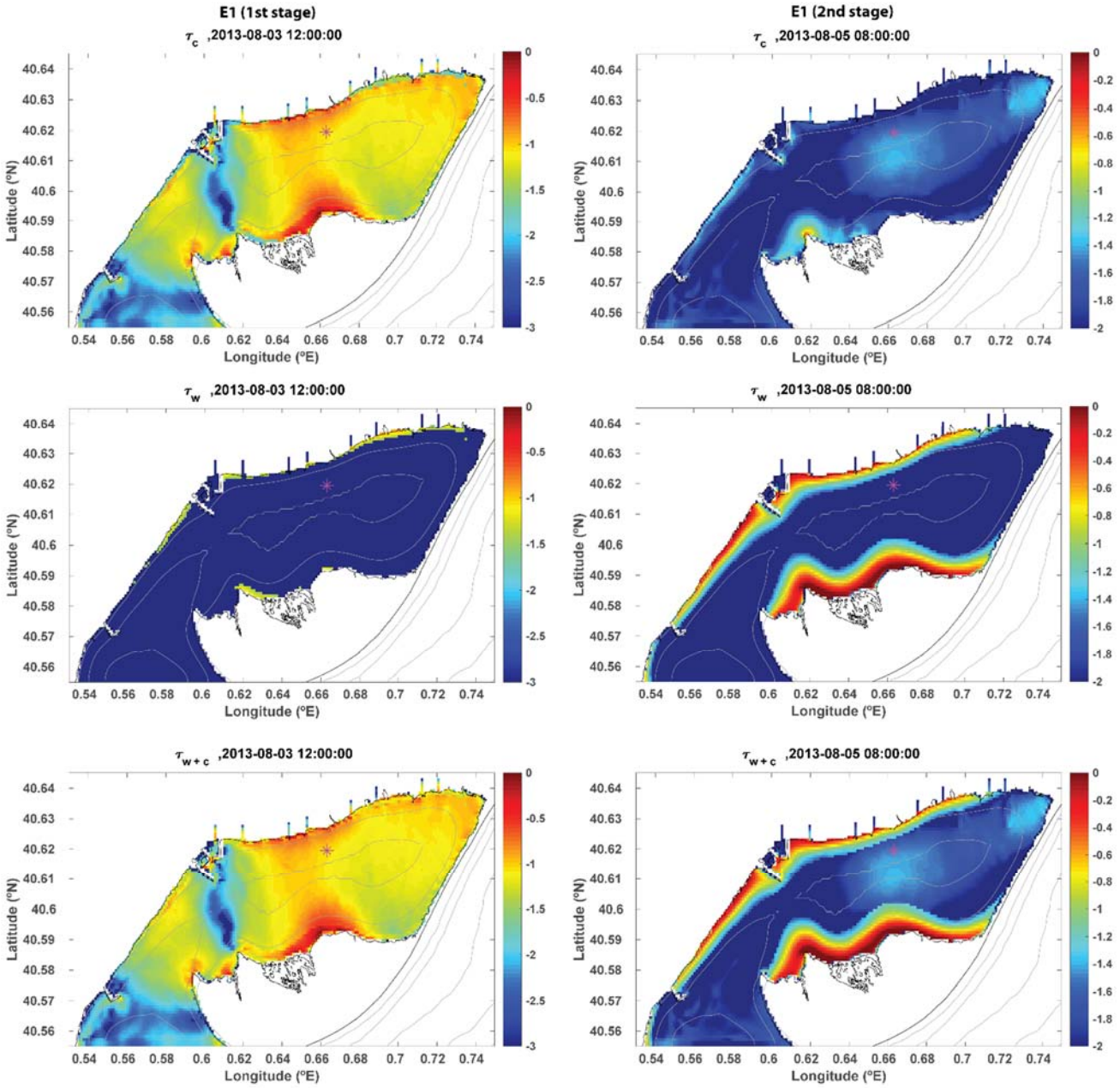

Figure 5: Current-induced bottom stress (τ_c), wave-induced bottom stress (τ_w) and combined wave-current bottom stress (τ_{wc}).in the Alfacs Bay during the first stage of the episode E1 (i.e. seiche; left panels) and the second stage of the episode E1 (i.e. sea breeze; right panels). The A2 station is shown in magenta. Isobaths are plotted in grey solid lines in 3 m intervals from 3 m to 12 m. Note that for clarity, the bottom stresses are plotted in log10 scale and the vertical range differs between both bottom stress distributions.

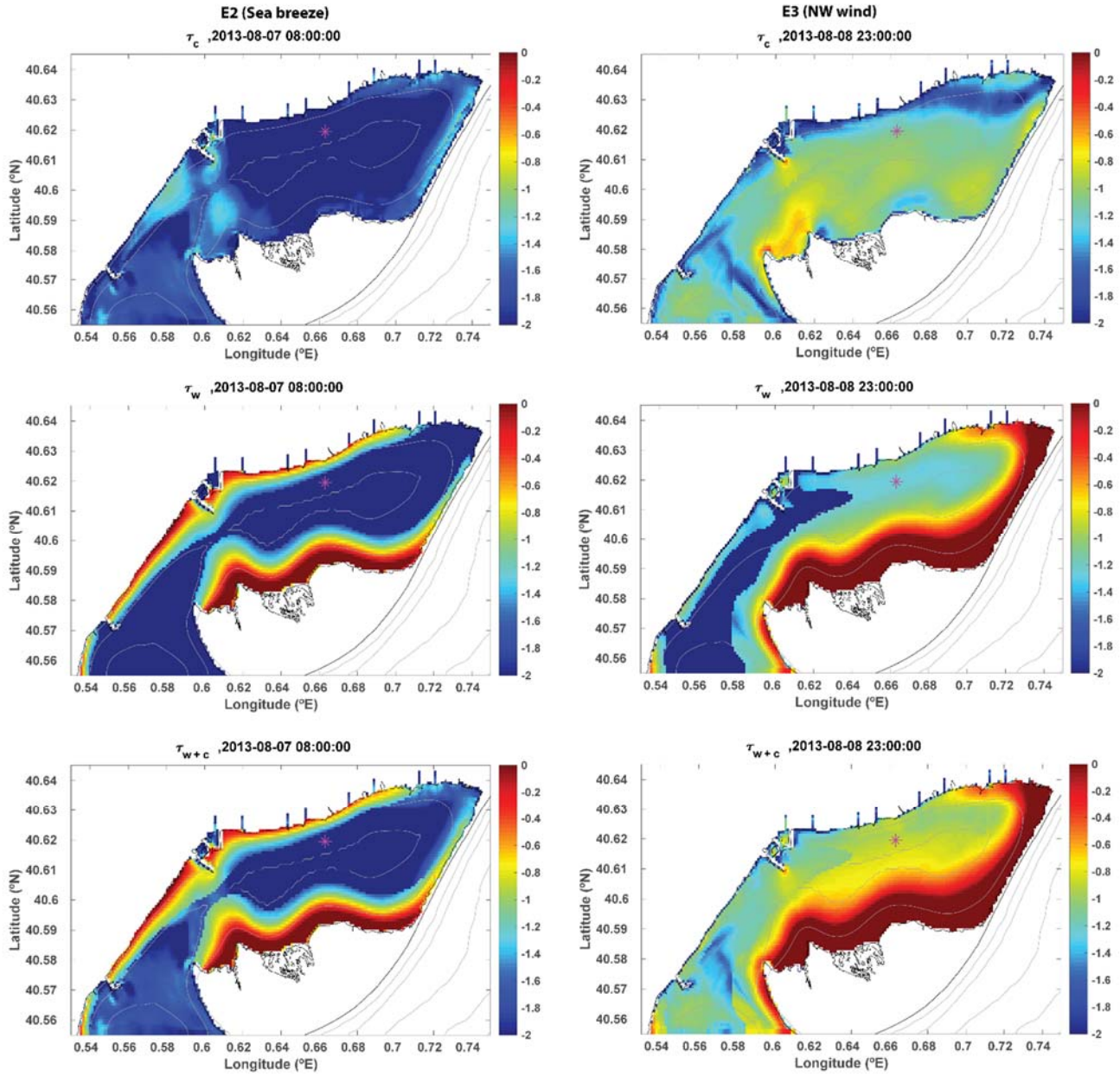

Figure 6: Current-induced bottom stress (τ_c), wave-induced bottom stress (τ_w) and combined wave-current bottom stress (τ_{wc}).in the Alfacs Bay during the first stage of the episodes E2 (left) and E3 (right). The A2 station is shown in magenta. Isobaths (in grey) are plotted in grey solid lines in each 3 m intervals from 3 m to 12 m. Note that for clarity, the plot scale is transformed in log10 scale and the vertical range differs between both bottom stress distributions.

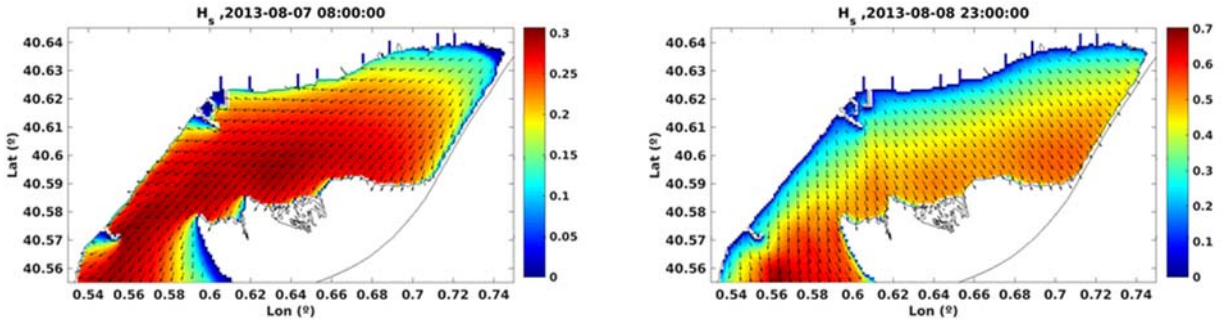

Figure 7: Wave field for the episode E2 (sea-breeze; left) and E3 (NW wind; right). The colours represent significant wave heights in meters and black arrows the direction of propagation. Note that the value ranges of colourbars are different.

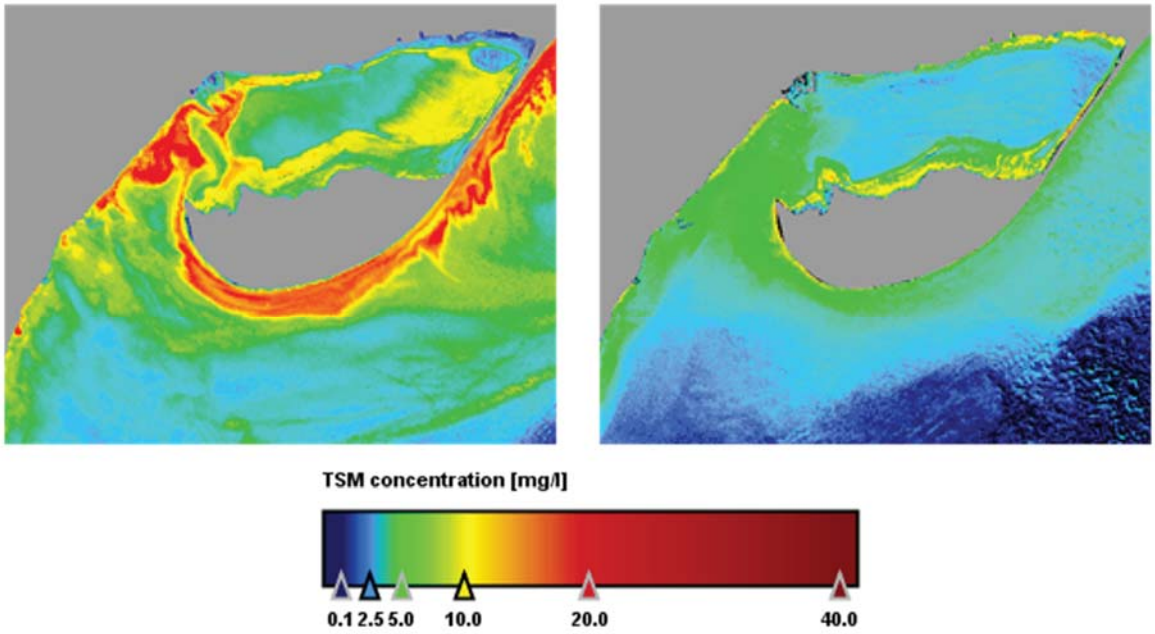

Figure 8: Total Suspended Matter (TSM in mg per 1iter) obtained from Sentinel-2 imagery for the Alfacs Bay for two different conditions: NW winds (left; 27th of December 2017) and calm conditions (right; 15th of February of 2018).